Scalar model for plasma turbulence

J. L. Ottinger and D. Carati
Service de Physique Statistique, Plasmas et Optique Non-Linéaire,
Faculté des Sciences, Université Libre de Bruxelles, Campus Plaine, Code Postal 231, B-1050 Bruxelles, Belgium
(Received 6 January 1993)

A shell model is proposed to study the Hasegawa-Mima equation [Phys. Fluids **21**, 87 (1978)] describing the electric-potential fluctuations in microturbulent plasmas. The similarities with two-dimensional hydrodynamic turbulence are discussed. Both the direct cascade of enstrophy and the reverse cascade of energy are investigated. The power-law spectra related to these cascades as well as the fluxes and higher moments of the fluctuations are computed. These quantities appear to be in good agreement with both the usually accepted phenomenology and the multifractal model.

PACS number(s): 52.35.Ra, 47.27.−i, 05.45.+b

I. INTRODUCTION

The complete description of turbulent flow in a laboratory or in natural conditions does not seem possible in the current state of mathematical physics. In the case of plasma turbulence, the problem appears to be even more complicated, due to the coupling between the velocity and the electromagnetic fields. This explains why analytical results remain so rare. Furthermore, the turbulent phenomena are characterized by a wide range of relevant spatial scales. In Fourier space, a large number of modes thus has to be taken into account. Due to both the complexity of the nonlinear coupling terms and the enormous number of degrees of freedom, analytical calculations as well as numerical simulations appear to be very difficult to achieve.

Recently, shell models [1–7] have been introduced to get around this difficulty. These models are used to investigate the statistical properties of strongly turbulent flows. The aim of shell formalism is clearly not to describe the complete and exact dynamics of the turbulence. Only the universal properties can be obtained from these simple models. Instead of considering each Fourier mode as an independent variable, these models introduce a small number of variables which are assumed to describe the characteristic behavior of a large set of Fourier modes. Such sets usually consist of all the modes corresponding to a shell of wave vectors. Unfortunately it is impossible to derive exactly the evolution equations for the collective variables by starting from the original equation. They are thus modeled in order to be as similar as possible to the latter. As a consequence of their small number of variables, the numerical and analytical investigation of the shell models is simpler than the analysis of the original equations. Their study has shown that, despite their simplicity, those models reproduce the main properties of spectra in both hydrodynamic [2–4] and magnetohydrodynamic (MHD) [1] turbulence. One of the main interests of the shell models resides in the fact that nontrivial characteristics of the averaged quantities, which could find their origin in the evolution of complex spatial structures [8,9], are also described by the chaotic behavior of these global variables. This explains why it could be interesting to apply these methods to other kinds of turbulence. Indeed, the instabilities observed in plasma physics are not limited to the MHD turbulence that appears in the collision-dominated plasmas. In this work, we are particularly interested by the microturbulence generated by drift-wave instabilities. They appear when the self-consistent electric field has a significant influence on the plasma dynamics and are usually described by the velocity distribution function. Hasegawa and Mima [10] have proposed a simplified closed equation for the electric-field fluctuations. The Hasegawa-Mima (HM) equation will be the starting point of our study. Of course, this equation is itself a simplified version of the complete set of equations describing the plasma dynamics. However, it is usually considered as a reasonable approximation to describe drift-wave turbulence. Moreover, it will be shown that its fairly simple structure lends itself easily to the shell-model formalism. We also note that the microturbulence could be the source of important fluxes of both energy and matter in magnetically confined plasmas in tokamaks [11]. It is then very important to develop simple approaches that should improve our understanding of the experimental conditions needed to perform controlled thermonuclear fusion in magnetically confined plasmas.

Our goal is then to investigate the statistical properties of the HM equation briefly presented in Sec. II by using the shell-model ideas. The first part of this work is devoted to the elaboration of the shell model related to the HM equation. We explain in Sec. III the arguments used to derive this shell model. They are very similar to those invoked by Yamada and Ohkitani [2] for the two-dimensional (2D) Navier-Stokes equation: enstrophy and energy conservation, required similitude of structure between the original equation and the model, etc. Some motivations for the introduction of this model are presented in Sec. IV. The second part of this work consists in testing the validity of the shell model. We show that both the energy and enstrophy spectra behave like power laws with characteristics that are in good agreement with the direct simulations of the HM equation. In a third step, we use the shell model to estimate quantities that are more difficult to obtain from experiments or from direct simulations. For example, higher-order mo-

ments of the electric potential fluctuations ($\langle \delta\phi^n \rangle$, with $n > 2$) are computed. We also obtain the wave-vector dependence of the energy transfer from small to large scales and similar results for the direct enstrophy cascade. Two ranges of wave vectors with different properties have been considered. In Sec. V we investigate the large-wave-vector range in which the HM model is equivalent to the two-dimensional Navier-Stokes (NS) equation for an incompressible inviscid fluid. Simulations corresponding to the small-wave-vector range are discussed in Sec. VI. Some general considerations concerning shell models and the existence of fixed points related to the cascades are pointed out in Sec. VII.

II. HASEGAWA-MIMA EQUATIONS FOR DRIFT-WAVE TURBULENCE

A. Model equations

The Hasegawa-Mima model [10] was introduced to describe a strongly turbulent two-dimensional plasma with cold ions. In such plasmas, the ions are considered as quasi-immobile while the electrons follow very intricate trajectories which can be seen as a combination of different kinds of motion: Along the magnetic field, the equilibrium is quickly reached [12] and the inertial motion is not perturbed over rather large scales. In the plane perpendicular to the magnetic field, the motion is decomposed into a fast gyration around the guiding center and a slow drift. In the HM model, two kinds of drift motion have to be considered: the electromagnetic and the polarization drifts, respectively, described by the velocities

$$\mathbf{v}_E = -\boldsymbol{\nabla}_\perp \phi \times \mathbf{B}/B_0^2 \tag{1}$$

and

$$\mathbf{v}_p = \frac{1}{\omega_{ci} B_0}\left[-\frac{\partial}{\partial t}\boldsymbol{\nabla}_\perp \phi - (\mathbf{v}_E \cdot \boldsymbol{\nabla}_\perp)\boldsymbol{\nabla}_\perp \phi\right] , \tag{2}$$

where t is the time and $\boldsymbol{\nabla}_\perp$ is the gradient in the plane perpendicular to the magnetic field. We work in the shearless slab geometry, where the magnetic field is constant in direction and intensity: $\mathbf{B} = B_0 \mathbf{1}_z$. Here $\mathbf{1}_z$ denotes the unit vector in the z direction. We have also introduced the ion-cyclotron frequency, $\omega_{ci} = eB_0/m_i$ ($-e$ is the electron charge and m_i the ion mass) and the fluctuation of the electrical potential ϕ. In the adiabatic approximation, this fluctuation obeys the Boltzmann distribution. It is related to the charge density n by the quasineutrality condition

$$n/n_0 = e\phi/T_e , \tag{3}$$

where n_0 is the equilibrium density of electrons and T_e is the electronic temperature.

To extract the long-time behavior of the electrons, it is usual to make the drift approximation consisting of an average over their fast gyration. The equation for the charge density reads then

$$\frac{\partial n}{\partial t} + \boldsymbol{\nabla}_\perp \cdot [n(\mathbf{v}_E + \mathbf{v}_p)] = 0 . \tag{4}$$

Relations (1) and (3) imply that the velocity $\mathbf{v}_E$ does not contribute to Eq. (4) because $\boldsymbol{\nabla}_\perp \cdot (n\mathbf{v}_E) = 0$. By using Eqs. (2)–(4), the evolution equation for ϕ in Fourier space reads

$$\frac{\partial \phi_{\mathbf{k}}(t)}{\partial t} + i\,\omega_{\mathbf{k}}^* \phi_{\mathbf{k}}(t) = \frac{1}{2} \sum_{\substack{\mathbf{k},\mathbf{k}',\mathbf{k}'' \\ \mathbf{k}=\mathbf{k}'+\mathbf{k}''}} \tilde{\Lambda}_{\mathbf{k},\mathbf{k}',\mathbf{k}''}\, \phi_{\mathbf{k}'}(t)\, \phi_{\mathbf{k}''}(t) . \tag{5}$$

The fluctuation $\phi(\mathbf{x}, t)$ is expanded in a spatial Fourier series in the plane perpendicular to $\mathbf{B}$:

$$\phi(x, y, t) = \frac{1}{2} \sum_{\mathbf{k}} [\phi_{\mathbf{k}}(t)\, e^{i\mathbf{k}\cdot\mathbf{x}} + \text{c.c.}] , \tag{6}$$

where $\mathbf{x} = (x, y)$ and $\mathbf{k} = (k_x, k_y)$. The coupling matrix elements $\tilde{\Lambda}_{\mathbf{k},\mathbf{k}',\mathbf{k}''}$ are given by

$$\tilde{\Lambda}_{\mathbf{k},\mathbf{k}',\mathbf{k}''} = \frac{1}{1+k^2}(\mathbf{k}' \times \mathbf{k}'') \cdot \mathbf{1}_z [(k'')^2 - (k')^2] . \tag{7}$$

In the linear term, the drift-wave frequency is given by

$$\omega_{\mathbf{k}}^* = \frac{-k_y T_e \partial(\ln n_0)/\partial x}{eB_0(1+k^2)\omega_{ci}} . \tag{8}$$

As usual, the space variable x in n_0 is assumed to refer to the slow spatial dependence of macroscopic quantities in the direction $\mathbf{1}_x$ perpendicular to the magnetic field. In Eq. (5), t and $\mathbf{x}$ are dimensionless variables expressing the time in units of ω_{ci} and the space in units of an effective gyroradius $\rho_s = \frac{c_s}{\omega_{ci}}$. Here, c_s denotes the ion sound speed given by $(T_e/m_i)^{1/2}$.

B. Relation with the 2D Navier-Stokes equation

As already pointed out by Hasegawa and Mima [10], in the range of wave vectors $k \gg 1$ Eq. (5) is equivalent to the NS equation for a two-dimensional incompressible and inviscid fluid:

$$\left(\frac{\partial}{\partial t} + \mathbf{v} \cdot \boldsymbol{\nabla}\right)\mathbf{v} = -\boldsymbol{\nabla} p , \tag{9}$$

$$\boldsymbol{\nabla} \cdot \mathbf{v} = 0 , \tag{10}$$

where $\mathbf{v}$ is the two-dimensional velocity field and p represents the hydrodynamic pressure.

Due to the incompressibility condition (10), the velocity derives from a scalar potential: $\mathbf{v} = \boldsymbol{\nabla} \times (\psi \mathbf{1}_z)$. By taking the curl of Eq. (9), we obtain

$$\left(\frac{\partial}{\partial t}\right)\boldsymbol{\nabla}_\perp^2 \psi - (\boldsymbol{\nabla}\psi \times \mathbf{1}_z \cdot \boldsymbol{\nabla})\boldsymbol{\nabla}_\perp^2 \psi = 0 . \tag{11}$$

In Fourier space, Eq. (11) reads

$$\frac{\partial \psi_{\mathbf{k}}(t)}{\partial t} = \frac{1}{2} \sum_{\substack{\mathbf{k},\mathbf{k}',\mathbf{k}'' \\ \mathbf{k}=\mathbf{k}'+\mathbf{k}''}} \tilde{\Lambda}^{\mathrm{NS}}_{\mathbf{k},\mathbf{k}',\mathbf{k}''} \psi_{\mathbf{k}'}(t) \psi_{\mathbf{k}''}(t) \ , \tag{12}$$

where

$$\tilde{\Lambda}^{\mathrm{NS}}_{\mathbf{k},\mathbf{k}',\mathbf{k}''} = \frac{1}{k^2} (\mathbf{k}' \times \mathbf{k}'') \cdot \mathbf{1}_z [(k'')^2 - (k')^2] \ . \tag{13}$$

If $k \gg 1$ the HM equation for an homogeneous plasma reduces to the NS equation for the scalar potential. Within this limit, the drift frequency becomes negligible and the nonlinear terms defined by the coupling matrices $\tilde{\Lambda}_{\mathbf{k},\mathbf{k}',\mathbf{k}''}$ (7) and $\tilde{\Lambda}^{\mathrm{NS}}_{\mathbf{k},\mathbf{k}',\mathbf{k}''}$ (13) are equal.

Let us notice that two important quantities are conserved by the HM equations: the electric energy

$$E = \sum_{\mathbf{k}} |\phi^2_{\mathbf{k}}|(1 + k^2) \tag{14}$$

and

$$Z = \sum_{\mathbf{k}} |\phi^2_{\mathbf{k}}|(1 + k^2)k^2 \ . \tag{15}$$

Because these quantities correspond to the kinetic energy and the enstrophy in the 2D NS equation, respectively, we are using the same vocabulary to denote E and Z in what follows. We shall discuss in the following sections the influence of these invariants.

III. SHELL MODEL FOR THE HM EQUATION

The shell models [1–7] were introduced to investigate the main properties of fully developed turbulence starting from very simplified equations. Instead of starting directly from the complete equations (NS, MHD, HM, etc.), the shell models only consider a small number of collective variables assumed to mimic the essence of the turbulent dynamics.

The Fourier space is then divided in shells around the origin. Each shell has a width g times greater than the previous one and includes all the wave vectors such that $k_0 g^{n-1/2} \leq k < k_0 g^{n+1/2}$. The parameter g is a free parameter of the model. Its choice will be discussed in Sec. VII. The characteristic wave vector length of a shell is given by

$$k_n = k_0 \ g^n \ , \tag{16}$$

and all information given by the modes $\phi_{\mathbf{k}}$ of the shell is assumed to be given by a single complex variable ϕ_n.

Unfortunately, due to the nonlinearity in the equation for $\phi_{\mathbf{k}}$, it is impossible to derive an exact equation for the collective variables ϕ_n. They are modeled in such a way that the main characteristics of the original equations are preserved. For the HM model, we choose the following equations:

$$\frac{\partial \phi_n}{\partial t} = i\omega_n \phi_n + \sum_{n',n''} \Lambda_{k_n,k_{n'},k_{n''}} \phi^*_{n'} \ \phi^*_{n''} + f_n - d_n \ \phi_n, \tag{17}$$

where ϕ^*_n is the complex conjugate of ϕ_n. Let us make the following remarks about Eq. (17).

(i) Each equation contains nonlinear terms which correspond to the convolution term. The matrix element $\Lambda_{k_n,k_{n'},k_{n''}}$ introduces a coupling between the shell variables labeled n, n', and n''. Such a coupling is the guess of what the couplings between all wave vectors $\mathbf{k}$, $\mathbf{k}'$, and $\mathbf{k}''$ belonging to the shells n, n', and n'' should be in the original HM equation. Its structure is chosen to mimic as much as possible the HM nonlinearity. Particularly, the shell equations are required to have the same k dependence as the original equation. This is the case if

$$\Lambda_{k_n,k_{n'},k_{n''}} = \alpha_{n,n',n''} \frac{1}{1 + k_n^2} (k_{n'} k_{n''})[k^2_{n''} - k^2_{n'}] \ . \tag{18}$$

The $\alpha_{n,n',n''}$ are of the order of unity and are chosen in such a way that the complete nonlinear term conserves both the total energy and the total enstrophy in the shell model:

$$E = \sum_{n=1}^{N} |\phi^2_n|(1 + k_n^2) \ , \tag{19}$$

$$Z = \sum_{n=1}^{N} |\phi^2_n|(1 + k_n^2)k_n^2 \ . \tag{20}$$

These quantities have to be compared with (14) and (15). A more complete analysis of the construction of the nonlinear term is given in Sec. VII.

(ii) In order to compare our results with previous works, we are using the usual locality assumption about the interactions in the Fourier space. The most important contribution in the nonlinear term of Eq. (5) is then assumed to originate from the triads $\{\mathbf{k}_1, \mathbf{k}_2, \mathbf{k}_3\}$ such that the three lengths k_1, k_2, and k_3 are of the same order. In the shell model, this implies that the only triplets $\{n, n', n''\}$ to be kept in Eq. (17) are $\{n, n+1, n+2\}$, $\{n-1, n, n+1\}$, and $\{n-2, n-1, n\}$. The equations are then given by

$$\frac{\partial \phi_n}{\partial t} = i\omega_n \phi_n + a_n \ \phi_{n-1} \ \phi_{n-2} + b_n \ \phi_{n-1} \ \phi_{n+1} + c_n \ \phi_{n+1} \ \phi_{n+2} + f_n - d_n \phi_n \ . \tag{21}$$

Using the definitions (16) and (18), we find

$$\begin{aligned} a_n &= \frac{\alpha}{1 + k_n^2} \ k_{n-2} \ k_{n-1} \ (k^2_{n-1} - k^2_{n-2}) \\ &= \frac{\alpha k_n^4}{1 + k_n^2} \ \frac{g^2 - 1}{g^7} \ , \\ b_n &= \frac{\beta k_n^4}{1 + k_n^2} \ \frac{g^4 - 1}{g^2} \ , \\ c_n &= \frac{\gamma k_n^4}{1 + k_n^2} \ (g^2 - 1) \ g^5 \ . \end{aligned} \tag{22}$$

The conservation of energy and enstrophy implies the following relations:

$$\beta = -\frac{\alpha}{g}, \quad \gamma = \frac{\alpha}{g^2} \ . \tag{23}$$

(iii) The frequency $\omega^*_{\mathbf{k}}$ (8) is clearly anisotropic in the perpendicular plane (k_x, k_y). Such a term is not easily described in the spirit of shell models. A possible solution would be to introduce a frequency with a similar but isotropic k dependence:

$$\omega_n = \frac{-k_n}{(1+k_n^2)} \frac{T_e\ \partial(\ln n_0)/\partial x}{eB_0\omega_{ci}} = \frac{-k_n}{(1+k_n^2)}\omega_0^* \ . \quad (24)$$

However, we are simply neglecting this term in the numerical simulations. Due to the k dependence of $\omega^*_{\mathbf{k}}$, such an approximation is certainly justified within both the very-large- and the very-small-k limits. It is not the case in the range around $k \sim 1$.

(iv) The external forcing term corresponds to an energy input in the system. It is assumed to occur in a very restricted range of wave vectors consisting of two successive shells labeled f and $f+1$. The characteristic length scale of the forcing is then approximately $1/k_f$. In the numerical simulations, we have chosen

$$f_n = j_0(\delta_{n,f} + \delta_{n,f+1}) \ , \quad (25)$$

where j_0 is a control parameter and $\delta_{i,j}$ is the Kronecker symbol.

(v) In order to prevent a continuous growth of energy and to keep the system in a stationary state, we also introduce dissipative terms that are neglected in the HM model. Indeed, at the laboratory scale as well as at microscopic scales, dissipation mechanisms always exist. The form of the dissipative terms is not important here because most of the analysis is made in the range of wavelengths where they do not influence the dynamics. Their role is to ensure the total dissipation of the input energy and enstrophy at the limits of our domain. For that purpose we take

$$d_n = \nu k_n^4 + \nu' k_n^{-6} \ , \quad (26)$$

where ν (ν') is the control parameter for the high- (low-) k region of the spectrum. The rapid increase of the dissipation at the edges of the domain allows us to reduce the number of modes where the dissipation influences the dynamics. We are then able to observe inertial ranges below and behind the forcing without keeping too many variables. The k^4 law describing the high-k viscosity was already used in the direct simulations of the 2D NS or HM equation [9,13,14]. The law describing the dissipation at low k is more difficult to justify because it is related to the large scales and depends thus on the geometry of the reactor, on edge phenomena. Other values for the exponent of k (-8 and -3 instead of -6) in this dissipation term were tested and no significant modification to the results appears in the cascade range.

The set of equations (17)–(26) defines the Hasegawa-Mima shell equations, which are used in the following sections.

IV. MOTIVATIONS

As already mentioned in the preceding section, it is generally impossible to derive from a nonlinear partial differential equation a set of exact shell equations. In that sense, any shell equation must be considered as a simplified model. It is usually made plausible by the great similarity between its structure and the one of the original equation. Of course, the applicability of such models reducing the number of variables from billions to less than a hundred may appear questionable. This is particularly true in the turbulence regimes where the large number of excited length scales is often emphasized. Moreover, a large amount of information is lost when a partial differential equation is modeled by shell equations. For all these reasons, it is important to address the questions "what is gained by using the shell model instead of the original equation and why can we be confident in the results?"

Before we discuss these points we would like to make clear the main differences between the shell models and the subgrid-scale models [15]. The latter are derived by modeling the small-scale phenomena that are usually assumed to be statistically homogeneous, stationary, and isotropic. The resulting equations are still nonlinear partial derivative equations with a cutoff in wave vector that reduces the number of Fourier modes. Consequently, they can be used to investigate the influence of the geometric characteristics of the experimental setup on the macroscopic properties of the flow. However, they lose their interest if one tries to use them to compute the dynamics of Fourier modes in a very large range of wave vectors. On the other hand, shell models are derived by modeling the dynamics of collective variables summarizing the relevant information of a shell of wave vectors. By definition, they are unable to reproduce any phenomena related to the geometry of the flow. However, they are assumed to describe the statistical and generic properties of a turbulent system for wave vectors that are not influenced by the boundary conditions or by the initial conditions.

Let us now explain why we believe that the statistics of the shell model could be a good approximation of the HM equation (once again, it must be confessed that no rigorous proof of this fact can be provided). First, we recall that the shell model derived for the Navier-Stokes equation has been shown to reproduce surprisingly well the universal statistics of both the 2D and the 3D turbulence [2–4,16]. Because we have followed a very similar procedure to derive the present shell model, their is no evident reason to believe that it will fail in the determination of the statistics of the drift-wave turbulence described by the HM equation. Second, it is shown in the following sections that the spectra of both the energy and the enstrophy computed by the shell model fit very well the direct simulation results [13,14]. Consequently, the shell model seems to be able to reproduce the very basic properties of the drift-wave turbulence. We then make the guess that it is also valid to investigate less conventional characteristics that are not so easy to obtain by direct simulation.

At this point, it is also important to stress why the shell models could be more useful than the original equation to investigate the statistics of turbulence, particularly in the case of the HM equations. Of course, consisting of a set

of simple dynamical equations, the numerical integration of the shell model is by far easier than the direct simulation of the HM equation. This is a trivial establishment that has nontrivial consequences. For example, by integrating the model over a very large time, the statistics of the shell variables can be determined in a very accurate way. Particularly, the high moments of the electric potential fluctuation ($\langle|\phi|^n\rangle$) can be computed until $n \approx 10$ [3,4,16]. Such values certainly cannot be reached by using the direct simulation of the HM equation. We have also computed the fluxes of energy and enstrophy, quantities for which estimation cannot be easily obtained by dimensional analysis as it is usually done for the spectra. In particular, we are showing that the fluxes behave very differently for scales that are larger than the characteristic length of energy injection and for scales that are smaller than this length. This is in agreement with the usual two cascades picture of 2D turbulence.

Let us briefly anticipate the final discussion (Sec. VI) to motivate further this work by two prospectives of the method. First, the simplicity of the shell-model equation should allow some analytical investigations that would probably be impossible for the original equation. Second, these models may play a large part in the understanding of the anomalous transport coefficients. Indeed, the relations between the thermodynamical fluxes and forces are usually dependent on the correlation between different fluctuations, i.e., precisely the quantities that can be easily computed in the shell-model formalism.

V. RESULTS IN THE NAVIER-STOKES RANGE

As discussed in Sec. II, the HM model is equivalent to the 2D incompressible and inviscid NS equations within the large-k limit. For that reason, the large wave vectors are said to correspond to the Navier-Stokes range. Here, we are investigating this NS range.

Two types of simulations were made with $g = 2$, $N = 30$ (run A) and $g = (1+\sqrt{5})/2$, $N = 40$ (run B). The reason for these choices is explained in Sec. VII. In both cases the wave-vector range is approximately the same: $k_0 = 1 \lesssim k \lesssim 10^9$ (the inertial range begins in these conditions at $k \sim 10$). The simulations may thus be compared to each other. The results presented in this section correspond to run A. They will be followed by the values corresponding to the run B, given between brackets, if they are different. The dissipation is defined by the values $\nu = 10^{-28}$ and $\nu' = 1000$ in (26). The free parameter α in the nonlinear terms (22) and (23) is chosen $\alpha = g^2$. The forcing term (25) acts on the central mode of the domain: $f = 14$ [$f = 20$], i.e., $k \sim 10^4$, and its intensity is determined by $j_0 = 0.01$.

Both runs are made with a fourth-order Runge-Kutta integrator with a variable time step chosen of the order of 1/20 of the fastest time scale of the variables ($dt \sim 5\times10^{-4}$). Typical values of the time scales of the different modes are

$$\tau(k_i) = \left| \frac{\langle|\phi_i{}^2|\rangle^{1/2}}{\partial\phi_i/\partial t} \right|, \tag{27}$$

where $\langle a\rangle$ is the average value of a. These values are shown in Fig. 1. The averages are taken over long times ($T \sim 200$).

In order to make easier the comparison between the shell variables and the Fourier-space variables, let us define the relations between the total energy, the energy spectrum, and the potential fluctuation spectrum. First, the relation between the energy spectrum $E(k)$ and the total energy is given by

$$E = \int_0^\infty dk\ E(k)\ . \tag{28}$$

On the other hand, the total energy is also related to the electric potential fluctuations:

$$E = \int d\mathbf{k}\ |\phi_{\mathbf{k}}|^2\ (1+k^2) = \int_0^\infty dk\ 2\pi\ k\ \overline{|\phi_k|^2}\ (1+k^2)\ , \tag{29}$$

where $\overline{x_k}$ denotes the spatial average of $x(\mathbf{k})$ over the angular variable. Finally, the total energy can be expressed in terms of the shell variables:

$$E = \sum_i\ (k_{i+1} - k_i)\ E(k_i) = \sum_i\ k_i\ (g-1)\ E(k_i)\ , \tag{30}$$

and similarly

$$E = \sum_i\ k_i\ (g-1)\ 2\pi\ k_i\ |\phi_i|^2\ (1+k_i{}^2)\ . \tag{31}$$

By comparing (30) and (31) with (19), (28), and (29), one obtains

$$\begin{aligned} \langle E(k_i)\rangle &= \frac{1+k_i{}^2}{k_i\ (g-1)}\langle|\phi_i|^2\rangle\ , \\ \langle\overline{|\phi_{k_i}|^2}\rangle &= \frac{\langle|\phi_i|^2\rangle}{k_i{}^2 2\pi(g-1)}\ . \end{aligned} \tag{32}$$

Let us note that in the NS range, if in shell variables the spectrum scales like

$$\langle|\phi_i|^2\rangle \propto k_i^{-\epsilon}\ , \tag{33}$$

the Fourier space spectrum will scale like

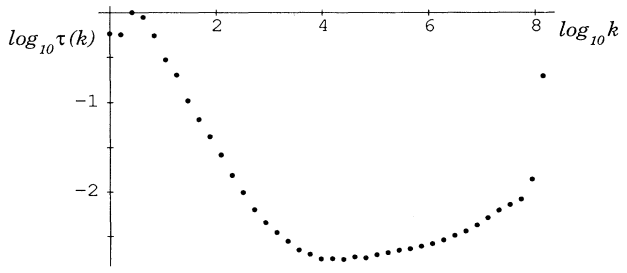

FIG. 1. Typical time scales for the Navier-Stokes regime as a function of the wave vector k. Time and space are dimensionless variables introduced in Sec. II.

$$E(k) \propto k^{-(\epsilon-1)}, \quad \overline{|\phi_k|^2} \propto k^{-(\epsilon+2)} . \tag{34}$$

The shell variable quantity $\langle|\phi_i|^2\rangle$ is shown in Fig. 2. Two regimes with different spectra $\langle|\phi_i|^2\rangle \propto k_i^{-\epsilon}$ are observed and the value of the exponent ϵ are

$$\epsilon = 4.29 \pm 0.01 \qquad [4.34 \pm 0.01] , \tag{35}$$

in the direct cascade (for the variables ϕ_i with $i \in \{17, 25\}$ $[\{22, 36\}]$) and

$$\epsilon = 1.90 \pm 0.12 \qquad [1.81 \pm 0.12] , \tag{36}$$

in the reverse cascade ($i \in \{4, 8\}$ $[\{5, 12\}]$). Kraichnan [17] has transposed Kolmogorov's arguments concerning the 3D turbulence to the 2D case. He predicted two regimes with characteristic exponents 4 and 8/3. The slopes corresponding to the Kraichnan-Kolmogorov (KK) values are also shown in Fig. 2.

The names "direct" and "inverse" cascades have not been chosen only because the power laws are roughly similar to the KK theory. Indeed, the directions of both the energy and enstrophy transfers have been calculated and are in good agreement with the usual phenomenology of direct and reverse cascades. Let us explain this point by considering the evolution of the energy contained in the region $k < k_i$, $E^<(i)$, which is given by three contributions:

$$\frac{\partial E^<(i)}{\partial t} = F_E^<(i) + D_E^<(i) + \Pi(i) , \tag{37}$$

where $F_E^<(i)$ and $D_E^<(i)$ respectively describe the total energy input and dissipation for the modes $< i$, and $\Pi(i)$ describes the flux of energy from the modes $\geq i$ to the modes $< i$. They respectively correspond to the forcing, the dissipation, and the nonlinear terms of (21). A similar equation can be written for the enstrophy contained in the region $k < k_i$:

$$\frac{\partial Z^<(i)}{\partial t} = F_Z^<(i) + D_Z^<(i) + \Omega(i) . \tag{38}$$

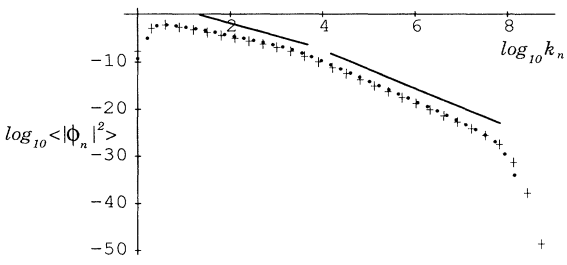

FIG. 2. Second-order moment of the fluctuations. The dots are obtained with a 40-mode simulation with $g = (1+\sqrt{5})/2$ and the crosses with 30 modes and $g = 2$. The forcing acts at $k \sim 10^4$. Two inertial ranges appear to the right and to the left of the forcing. The straight lines correspond to the Kraichnan-Kolmogorov's spectra, i.e., $k^{-8/3}$ and k^{-4}.

The nonlinear fluxes are given by

$$\Pi(i) = \frac{1}{2}\sum_{j=1}^{i}(1+{k_j}^2)\phi_j{}^* \frac{\partial^{\rm NL}\phi_j}{\partial t} + \text{c.c.} , \tag{39}$$

$$\Omega(i) = \frac{1}{2}\sum_{j=1}^{i}(1+{k_j}^2){k_j}^2\phi_j{}^* \frac{\partial^{\rm NL}\phi_j}{\partial t} + \text{c.c.} , \tag{40}$$

where $\frac{\partial^{\rm NL}\phi_i}{\partial t}$ denotes the contribution of the nonlinear terms in Eq. (17) for the time evolution of ϕ_i.

The average fluxes of energy and enstrophy are presented in Figs. 3 and 4. The flux properties are very different following the range of the wave vector. First, for the wave vectors smaller than k_f, the enstrophy flux is zero while the energy flux is negative and almost constant. This range is then associated to a reverse energy cascade without enstrophy transfer. On the other hand, the enstrophy flux is positive and constant while the energy flux is zero for the wave vectors larger than k_f. Such wave vectors correspond to a direct enstrophy cascade without energy transfer. This is in complete agreement with the KK theory for the 2D turbulence in neutral fluids. The range of shell variables used to evaluate the characteristic exponents for the scaling laws are, respectively, $\{17, 25\}$ $[\{22, 36\}]$ in the direct cascade and $\{4, 8\}$ $[\{5, 12\}]$ in the reverse cascade. They correspond to the ranges of wave vector where the fluxes are reasonably constant: $5 \times 10^4 \lesssim k \lesssim 10^7$ and $10 \lesssim k \lesssim 150$. The decrease of the fluxes for the smallest and the highest wave vectors is due to the dissipation phenomena modeled by d_n. We note that the enstrophy flux is more stable than the energy flux. This can be a consequence of the characteristic time scales profile presented in Fig. 1. Indeed, the time scales are smaller in the direct enstrophy cascade. The average is thus more reliable in this range.

We have also computed the structure function ξ_Q

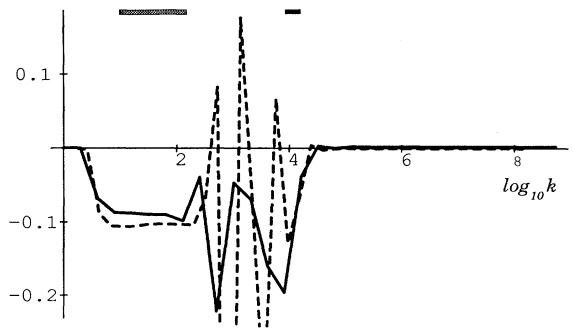

FIG. 3. The averaged flux of energy in the 30-mode simulation (full line) and 40-mode simulation (dashed line). The flux is zero after the forcing and negative before. The energy coming from the forcing, at $k \sim 10^4$ (in black above the figure) is dissipated at low k. The range of modes used for the calculation of the structure functions in the reverse cascade is shown in grey above the figure. It corresponds to the region where the flux of energy is "reasonably" constant.

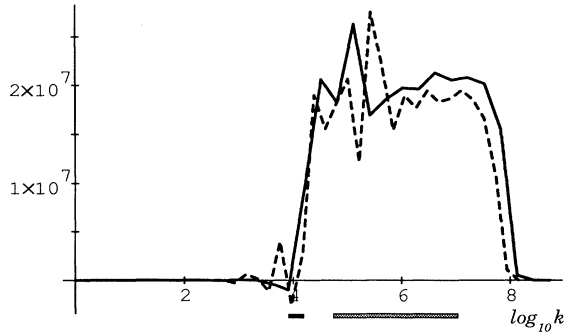

FIG. 4. The averaged flux of enstrophy in the 30-mode simulation (full line) and 40-mode simulation (dashed line). The flux is zero before the forcing range ($k \sim 10^4$, in black under the k axis) and positive before. The enstrophy coming from the forcing is dissipated at high k. The range of modes used for the calculation of the structure functions in the direct cascade is shown in grey under the k axis. It corresponds to the region where the flux of enstrophy is reasonably constant.

[3,4,16,18] which describes the velocity moment according to the definition $\langle |\phi_n|^Q \rangle \propto k_n^{-\xi_Q}$. The dimensional analysis predicts that the structure functions are given by $\xi_Q = 2Q$ in the direct enstrophy cascade and by $\tilde{\xi}_Q = 4/3\ Q$ in the reverse energy cascade. These slopes and the results of the simulations are shown in Fig. 5. The structure functions we observe with our model are $\xi_Q = \alpha_D Q$ and $\tilde{\xi}_Q = \alpha_R Q$ in the direct and the reverse cascades, respectively. The values of the slopes are

$$\begin{aligned} \alpha_D &= 2.13 \pm 0.01 \qquad (2.15 \pm 0.01)\ , \\ \alpha_R &= 0.95 \pm 0.06 \qquad (0.9 \pm 0.05)\ . \end{aligned} \tag{41}$$

Such structure functions have been studied in the 3D case [3,4] and a nonlinear deviation to the Kolmogorov laws has been observed. Such a deviation should be related to the singularities of the velocity gradient and to

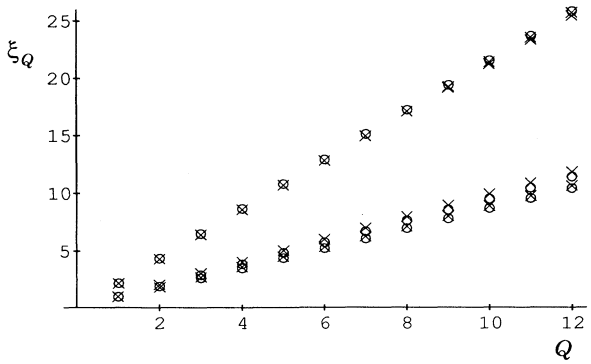

FIG. 5. The structure functions in the 30- (crosses) and 40- (dots) mode simulations in the direct and the reverse cascade. When the gap between the lowest and the highest values is large enough, these two values are shown. The functions are linear in Q. The choice of the numbers of modes does not influence the result.

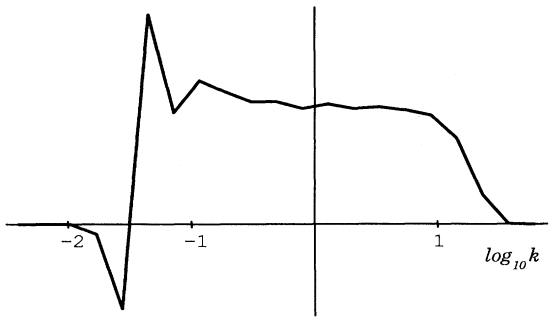

FIG. 6. The flux of enstrophy in the small-wave-vector regime, in arbitrary units. The forcing acts at $k \sim 0.02$. A range of wave numbers where the enstrophy flux is almost constant clearly appears. This corresponds to the direct enstrophy cascade.

the multifractal structure of the set where the energy dissipation is concentrated; this deviation is in good agreement with the β models [3,4,19]. In the 2D case, the enstrophy conservation does not allow us to apply the β model's assumptions. The linearity of the functions ξ_Q in the two cascades seems coherent with the model. The multifractal analysis of the two-dimensional turbulence also predicts the linearity of the structure function [20].

VI. RESULTS IN THE SMALL-WAVE-VECTOR RANGE

In this section, we are considering the shell model (17)–(26) in a range including wave vectors around 1. In this case, the equivalence with the 2D NS equation does not hold and new phenomena could be observed. Particularly, Hasegawa and Mima expected a bell spectrum rather than a power law for the electric-potential fluctuation spectrum. However, this bell spectrum was never observed in direct numerical simulations of their model [13,14]. Our results exhibit scaling laws even in the small-wave-vector range, in agreement with the direct simulations. Moreover, the scaling exponents are almost the same as in the NS range.

The simulations were made with $g = (1 + \sqrt{5})/2$ and $N = 21$ for a wave-vector range given by $10^{-3} < k < 10^4$ ($k_0 = 0.004$). Both the direct enstrophy cascade and the reverse energy cascade may not coexist in the same region. The choice of the forcing range determine thus which one will be observed in the turning-point range $k \sim 1$. To compare our results with the Hasegawa-Mima paper, we force the system in the low-k region (on the third and fourth modes, $k \sim 0.02$), with an amplitude determined by $j_0 = 0.0001$. The dissipation mainly acts in the high-k region; $\nu = 5 \times 10^{-7}$. In the low-k region only the first and second modes are subject to dissipation. The free parameter α for the nonlinear terms (22) and (23) was chosen $\alpha = g^2$.

Preliminary runs have been done including a drift frequency (24), with $w_0^* = 2000$, 500, and 10. The results appear to be independent of this parameter. The drift

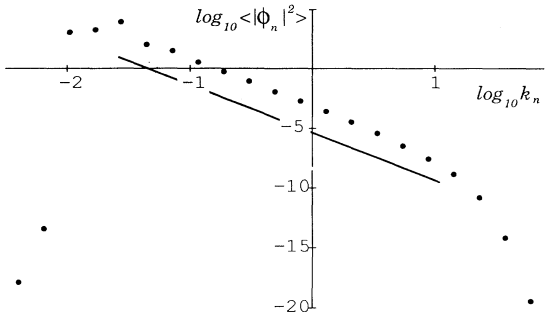

FIG. 7. The fluctuation spectrum in the small-wave-vector range exhibit a power-law behavior $\langle|\phi_i|^2\rangle \propto k^{-4.22}$. The straight line corresponds to the Kraichnan-Kolmogorov dimensional analysis ($\propto k^{-4}$).

frequency induces a mixing between the real part and the imaginary part of a shell mode, which does not modify the value of the moment of the fluctuation. In the simulation described in this section, we suppress the contribution of the drift-frequency term by assuming $w_0^* = 0$.

The behavior of the variables ϕ_k is very similar to the NS regime. We observe the direct enstrophy cascade (Fig. 6) and a power law (Fig. 7) for the potential fluctuation spectrum $\langle|\phi_i|^2\rangle \propto k^{-\epsilon}$ with

$$\epsilon = 4.22 \pm 0.15 \ . \tag{42}$$

Of course, the energy and enstrophy spectra are no longer given by a simple power law because of the factor $1 + k^2$. The structure function, shown in Fig. 8, is the same as in the NS range:

$$\xi_Q = \alpha Q \qquad \text{with } \alpha = 1.98 \pm 0.07 \ . \tag{43}$$

This clearly shows that scaling laws are valid for both $k < 1$ and $k > 1$. Particularly, we do not observe any bell profile for the fluctuation's spectrum, in agreement with the direct simulation of the HM model [13,14]. The value of the slope, a little steeper than 4, is in good agreement with the Fyfe-Montgomery simulations. Let us note that Crotinger and Dupree observe a slope steeper than ours, but their simulations are made in a different context: they describe the nonstationary turbulence which

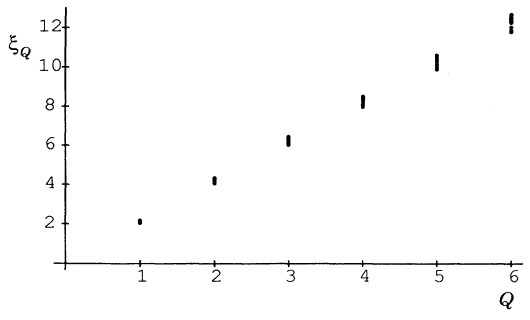

FIG. 8. The structure function in the small-k range. It appears to be linear with a slope equal to 1.98.

appears, without forcing, with an initial potential fluctuation spectrum far from the power-law spectrum.

VII. REMARKS ON THE CONSTRUCTION OF SHELL MODELS

The preceding sections clearly show that shell models are able to exhibit many interesting features of the strong turbulence, such as the existence of two different cascades. It is interesting to discuss what the essential ingredients of the model are and what the assumptions necessary to obtain the scaling laws are. Moreover, we would like to determine how the main results obtained from the shell equations depend on the parameters of the model.

Let us construct a shell model step by step, using as few restrictive hypotheses as possible. We start with a finite number of variables; we thus relate the field $\phi_{\mathbf{k}}$, defined on the continuous plane $\mathbf{k} = (k_x, k_y)$, to the set ${}^i\phi$, $i = 1, \ldots, N_{\text{tot}}$ defined on a certain grid $\{\mathbf{k}_i\}$ on the same plane. If the grid is symmetric with respect to the origin, one can find, for each i, an index $\bar{i}$ such that $\phi_i^* = \phi_{\bar{i}}$ (this corresponds to the condition $\phi_{\mathbf{k}}^* = \phi_{-\mathbf{k}}$). The time evolution of these variables is described by equations containing a forcing term, a linear term, and a nonlinear term:

$${}^i\dot{\phi} = F_i + L_i\,{}^i\phi + \sum_{j,l}^{N_{\text{tot}}} \Lambda^{ijl}\,{}^j\phi\,{}^l\phi \ , \tag{44}$$

with $\Lambda^{ijl} = \Lambda^{ilj}$. The nonlinear term is chosen in order to ensure the same conservation laws as the initial equations, i.e.,

$$E = \sum_i |{}^i\phi|^2(1 + k_i^2) = \text{C} \ , \tag{45}$$

$$Z = \sum_i |{}^i\phi|^2(1 + k_i^2)k_i^2 = \text{C}' \ . \tag{46}$$

It is easy to show that this implies

$$\Lambda^{ijl} = \Lambda^{\bar{j}li}\frac{1 + k_j^2}{1 + k_i^2}\,\frac{k_l^2 - k_j^2}{k_i^2 - k_l^2} \ . \tag{47}$$

At this stage there is not yet any shell structure in the equation. Such a structure arises if we impose a discrete scale invariance for the equations. Indeed, let us assume that both the grid $\{\mathbf{k}_i\}$ and the evolution equation for $\phi_{\mathbf{k}_i}$ are invariant for the change $k \to gk$. In this case, the grid has to consist of N_R rings all divided in the same way into N_A angular sectors. The variable associated with the grid structure will be denoted by ϕ_i^x, where i and x characterize the ring and the angular sector, respectively. Successive rings must have radius proportional to powers of g. The choice of g is free. The value 2 is probably preferred because of the picture of an eddy of size l broken in 2^d eddies of size $l/2$. In their more complex model for three-dimensional fluid turbulence, Eggers and Gross-

mann [21] construct a grid invariant under the transformation $k \to 2k$ and carefully take into account all the possible interacting triads. Equivalent models could be constructed with another factor for the invariance. In the spirit of shell models, where the variables are supposed to represent all the wave vectors of the shell, such a choice introduces spurious coupling. For example, wave vectors of lengths k, $2k$, and $4k$ are coupled, while no triads exist with these lengths. More realistic values of g are those such that $g^{n+2} \leq g^{n+1} + g^n$, i.e., $g \leq (1+\sqrt{5})/2$, the golden number.

The scale invariance in the equation for the shell model reflects a characteristic of the nonlinear term of the original equation. By rewriting (7)

$$\Lambda_{\mathbf{k},\mathbf{k}',\mathbf{k}''} = \frac{k^4}{1+k^2}\left(\frac{\mathbf{k}'}{k}\times\frac{\mathbf{k}''}{k}\right)\cdot\mathbf{1}_z\left[\left(\frac{k''}{k}\right)^2-\left(\frac{k'}{k}\right)^2\right] = H(k)\,G\left(\frac{\mathbf{k}'}{k},\frac{\mathbf{k}''}{k}\right), \tag{48}$$

one sees that the coupling matrix elements changes under the transformation $\mathbf{k} \to g\mathbf{k}$ only through $H(k)$. The coupling matrix for the variables ϕ_i^x should have the same property. This will be the case if Λ^{ijl} is a product of $H(k_i)$ and a function Θ depending only on the angular variables and the ratios k_j/k_i and k_l/k_i. This implies that the nonlinear term can be rewritten as follows:

$$^{\mathrm{NL}}\dot{\phi}_i^u = \sum_{j,l=1}^{N_R}\sum_{v,w=1}^{N_A}\Theta^{uvw}_{(i-j)(i-l)}\,H(k_i)\,\phi_j^v\phi_l^w\,, \tag{49}$$

with $\Theta^{uvw}_{ab} = \Theta^{uwv}_{ba}$.

The energy and enstrophy conservation leads to

$$\Theta^{\bar{u}vw}_{(i-j)(i-l)} = \Theta^{\bar{v}wu}_{(j-l)(j-i)}\frac{1+k_j^2}{1+k_i^2}\,\frac{k_l^2-k_j^2}{k_i^2-k_l^2}\,\frac{H(k_j)}{H(k_i)}\,. \tag{50}$$

With these simple assumptions, without any further considerations about the coupling constants $\Theta^{uvw}_{(i-j)(i-l)}$, we come to the following important conclusion: it is possible to find stationary solutions for Eq. (49) of the type

$$\phi_i^u = Ak_i^\epsilon, \tag{51}$$

if

$$H(k_i) = \frac{k_i^\delta}{1+k_i^2}\,. \tag{52}$$

There are two branches of solutions:

$$\epsilon = -\frac{\delta}{3}, \quad \epsilon = -\frac{\delta+2}{3}\,. \tag{53}$$

Note that if one chooses $\delta = 4$, in agreement with the original equation, these stationary solutions correspond to the usual KK direct and reverse cascades where the energy spectrum is given, respectively, by the power law

$$E(k) \propto k^{-3}, \quad E(k) \propto k^{-5/3}\,. \tag{54}$$

The shell model described in Sec. III is a particular case of the model described here. We have chosen $N_A = 1$ so that the variables u, v, and w disappear. Moreover, we restricted the shell coupling to local interaction, i.e., $\Theta^{uvw}_{(i-j)(i-l)} = 0$ if $|i-j| > 2$ or $|i-l| > 2$. The results (51)–(54) show that these restrictions are not necessary for obtaining the fixed points corresponding to the Kraichnan-Kolmogorov cascades. It could be interesting to analyze models using nonlocal couplings $(i, i+n_1, i+n_1+n_2), n_1 > 1$.

The shell variables described by Eqs. (17)–(26) do not remain close to the fixed points. Indeed, such fixed points are unstable and the system quickly reaches a chaotic regime. However, their existence could influence the dynamics of the system and, consequently, the observed spectra. We have shown in this section that the fixed points originate from the conservation laws and the assumed scale invariance in the simple shell model as well as in the more general equations with the nonlinear term (49) and angular dependence for the variables.

VIII. DISCUSSION

A shell model related to the Hasegawa-Mima model for the plasma drift-wave turbulence has been proposed. There were three objectives of the present work: the derivation of the shell model, the test of it in order to be sure that the basic characteristics of the HM equation are recovered, and its use to investigate new properties of the electric potential statistics. We have already explained that, as in the other applications of shell model, the derivation is based on plausibility arguments more than on a rigorous proof. The test has consisted in comparing the results of the model with some properties of the original equation that are obtained by other methods. Thus we chose to compute the spectra of energy and enstrophy in different ranges of wave vectors. The results presented in Secs. V and VI for these quantities appear to be in good agreement with the direct simulations and the usually accepted phenomenology. Having obtained these results, the model has been used to derive more complicated properties of the statistics such as higher-order moments and the transfer of energy and enstrophy.

We have first considered the range in which the HM model is equivalent to the 2D Navier-Stokes equation for an incompressible inviscid fluid. In the dimensionless variables introduced in Sec. II, such a range corresponds to $k \gg 1$. The numerical results exhibit the main properties of 2D turbulence. We observe a direct cascade of enstrophy and a reverse cascade of energy. Moreover, both the fluxes and the spectra of energy and enstrophy are in good agreement with the accepted phenomenology of 2D turbulence, described by the Kraichnan-Kolmogorov theory [17,18]. In that sense, the numerical results derived from shell model do not seem to depend on the equations. If two equations are equivalent (for instance, HM for $k \gg 1$ and 2D NS), the corresponding shell models will exhibit very similar results. This is a very important property showing the robustness of shell models. Moreover, we have shown that the results are almost independent of the shell width g, which is a free parameter in the

model.

The agreement between shell models and 2D turbulence (described by the Navier-Stokes equation or by the Hasegawa-Mima equation) deserves some comments. Indeed, recent experiments and simulations [8,9] have emphasized the dominant role of large-scale structures and collective phenomena in this kind of turbulence. As already noted, since the geometrical information of the flow is lost, the shell model is unable to describe the evolution of specific spatial structures. The success of shell models seems then to demonstrate that the particularities of the structures that appear in turbulent flow are unimportant to describe the statistical characteristics of the cascade ranges. However, the geometrical properties of large-scale structures should probably play a crucial role in the dissipation of energy at large scale due to the inverse energy cascade [20]. We have also investigated the small-k range, where Hasegawa and Mima expected to find a bell profile for the potential fluctuation spectrum. We do not observe such a profile and, in agreement with direct simulations of the HM equations, the shell-model spectra behave like power laws very similar to the direct cascade in the NS range. The transfer of energy from small scales to large scales vanishes and the enstrophy transfer is positive and almost constant. Moreover, the spectrum ($\propto k^{-4.22}$) is the same as in the large-wave-vector range.

The shell model was also used in both ranges to compute higher moments of the fluctuation $\langle|\phi|^n\rangle$ (until $n = 12$). This study was already made in the 3D NS turbulence case. A fine experiment of Anselmet *et al.* [16] has shown that the structure functions of a turbulent flow do not follow the linear prediction of the KK theory. These deviations are easily observed in shell-model simulations. They corroborate the existence of intermittency phenomena and of multifractality characteristics of the flow [20,19,3]. Of course, experimental results for higher-order moments are very difficult to obtain in 2D (or quasi-2D) turbulent systems such as atmospheric or oceanographic flow and strongly magnetized plasmas. Nevertheless, the theoretical arguments used in the 3D case, applied to the 2D case, are strongly modified by the enstrophy conservation and lead to the conclusion that even in the presence of intermittency, the KK prediction holds [20]. Our simulations confirm this prediction.

Finally, we have shown that the KK power-law spectra can be related to the fixed points of the shell-model equations. This establishment is valid for the HM shell model, but also for more complicated models including the vectorial structure of the Fourier space but keeping only a few modes. This kind of model was introduced in the 3D turbulence investigation by Grossman and Eggers [21] and provides an intermediate model between the complete equation and the shell model.

Let us end this discussion by some prospectives of the method. We have already mentioned that the simplicity of the shell-model equation should allow some analytical investigations that would probably be impossible for the original equation. Random-process methods [5] and small-dynamical-system techniques [6] have been applied recently to study the shell model for the Navier-Stokes equation. The results obtained analytically are then used to corroborate other theory by using a very different approach [19,20]. Another recent use of shell models concerns the modeling of the advection of a passive-scalar field in the 3D hydrodynamic turbulence [4]. Similar methods could be applied to investigate the transport in plasma: shell equations for both the charge (related to ϕ) and particle (n) density could provide statistical properties of the moments of these distributions, such as $\langle\phi\ \phi\rangle$ or $\langle\phi\ n\rangle$, which play an important role in the transport coefficients theory.

We are fully aware of the limitation of shell models, but we believe that they are a powerful tool to investigate some universal characteristics of turbulence statistics. Their chaotic behavior is rich in information that could not be analyzed through the resolution of the original equation.

ACKNOWLEDGMENTS

We are thankful to M.H. Jensen, G. Paladin, L. Biferale, and R. Balescu for useful discussions. One of us (D.C.) acknowledges financial support from the Fonds National de la Recherche Scientifique (FNRS, Belgium). The Service de Physique Statistique is part of the Association EURATOM-Etat Belge.

[1] C. Gloaguen, J. Léorat, A. Pouquet, and R. Grappin, Physica D **17**, 154 (1985).
[2] M. Yamada and K. Ohkitani, Phys. Rev. Lett. **60**, 983 (1988); Prog. Theor. Phys. **79**, 1265 (1988); **81**, 329 (1989); **84**, 415 (1990).
[3] M.H. Jensen, G. Paladin, and A. Vulpiani, Phys. Rev. A **43**, 798 (1991).
[4] M.H. Jensen, G. Paladin, and A. Vulpiani, Phys. Rev. A **45**, 7214 (1992).
[5] R. Benzi, L. Biferale, and G. Parisi, Physica D **65**, 163 (1993).
[6] D. Pisarenko, D. Courvoisier, U. Frish, and M. Vergassola (unpublished).
[7] L. Biferale, Phys. Fluids A **5**, 428 (1993).
[8] R. Benzi, G. Paladin, S. Paternello, P. Santangelo, and A Vulpiani, J. Phys. A **19**, 3771 (1986).
[9] J. McWilliams, J. Fluid Mech. **146**, 21 (1984).
[10] A. Hasegawa and K. Mima, Phys. Fluids **21**, 87 (1978).
[11] P. Liewer, Nucl. Fusion **22**, 543 (1985).
[12] J.B. Taylor and B. McNamara, Phys. Fluids **14**, 1492 (1971).
[13] D. Fyfe and D. Montgomery, Phys. Fluids **22**, 246 (1979).
[14] J.A. Crotinger and T.H. Dupree, Phys. Fluids B **4**, 2854 (1992).
[15] J. Smagorinsky, Mon. Weather Rev. **91**, 99 (1963).
[16] F. Anselmet, Y. Gagne, E.J. Hopfinger, and R.A. Antonia, J. Fluid Mech. **140**, 63 (1984).
[17] R.H. Kraichnan, Phys. Fluids **10**, 1417 (1967); J. Fluid

Mech. **47**, 525 (1971).
[18] H.A. Rose and P.L.Sulem, J. Phys. (Paris) **5**, 441 (1978).
[19] R. Benzi, G. Paladin, G. Parisi, and A. Vulpiani, J. Phys. A **17**, 3521 (1984).
[20] G. Paladin and A. Vulpiani, Phys. Rep. **156**, 147 (1987).
[21] J. Eggers and S. Grossman, Phys. Lett. A **156**, 444 (1991).